

Supplementary Materials for

Structure of Histone-based Chromatin in Archaea

Francesca Mattioli^{1†}, Sudipta Bhattacharyya^{2‡†}, Pamela N. Dyer¹, Alison E. White¹, Kathleen Sandman³, Brett W. Burkhardt², Kyle R. Byrne², Thomas Lee¹, Natalie G. Ahn¹, Thomas J. Santangelo^{2,4}, John N. Reeve³, and Karolin Luger^{1,4,5*}

correspondence to: Karolin.Luger@colorado.edu

This PDF file includes:

Materials and Methods

Figures S1-S6

Tables S1-S4

References (23-47)

Materials and Methods

Protein purification. Recombinant HMfB, HTkA wild type and mutants were induced, purified and quantified from *Escherichia coli* as described (13, 23)

DNA. The DNA molecule, SELEX-selected for high HMfB affinity (8) has the sequence 5'TATGAACCGTACTGTCGTCTGCGGCCTTTGATTATCAATTAAAGCGTTCTACGGCG TTTTGGATCGCTCAACGTGCGGAGCTAGATCTCA. The 5'-TA dinucleotide shown, and a 5'-TA on the opposite strand constitute single-stranded DNA extensions from the central 88 bp duplex DNA. Plasmid DNA was purified with a Qiagen Giga kit, and fragments were released by *NdeI* digestion.

Complex assembly for crystallization. Complexes were assembled in 100 mM KCl, 50 mM Tris·HCl (pH 8) by mixing increasing ratios of DNA to protein. After incubation at room temperature for 20 min, large scale preparations were purified by preparative gel electrophoresis [BioRad Prep Cell; (24)]. KCl was immediately added to the eluted fraction to a final concentration of 50 mM, and then aliquots of the complex were concentrated before incubation at 37°C, 55°C and 72°C for 30 min.

Crystallization. Crystals were obtained by vapor diffusion (sitting drop geometry). Purified complex (9.6 mg/ml) was mixed with an equal volume of 100 mM MgAc, 50 mM Na cacodylate, 10% PEG 400 (pH 6.5) under oil. Rod-shaped crystals (90 μ m diameter, ~230 μ m long), present after 10 days incubation at room temperature, were mounted in a loop, passed quickly through 100% glycerol, and frozen in liquid N₂.

Data collection. Data were collected on a Rigaku RU-H3R rotating anode generator equipped with an Osmic Confocal multilayer optics system and on an R-Axis IV image plate detector. They were indexed and reduced with XDS (25). Screw axes were determined by Pointless (26), followed by merging and scaling of the data using SCALA from the CCP4 suite (27).

Data analysis. Initial phasing by molecular replacement (MR) was performed using a single HMfB chain from the previously solved (HMfB)₂ crystal structure (1A7W) together with the structure of an 85 bp ds DNA molecule derived from the nucleosome (1AOI). The MR search was conducted with the assumption of a 6 histone to 1 DNA ratio. The initial data processing indicated P6/mmm Laue symmetry, but further solvent content analysis suggested twinning or pseudo-symmetry and led to reprocessing the data in P6, P321 and P312 point groups. PHASER (28) yielded a good MR solution in the P6₅ space group. The data were re-indexed in P6₅ and a further 40 cycles of rigid body refinement was carried out using Refmac5 (29). An analysis of the self-rotation function by Molrep (30) revealed the presence of 18 non-crystallographic two-fold symmetry vector peaks perpendicular to the crystallographic six-fold symmetry axis that likely led to the initial P6/mmm Laue symmetry. No twinning was detected for the merged P6₅ data using the unbiased L test and NZ test with Phenix (31) with an Xtriage multivariate Z score of 3.03. After rigid body refinement, the initial model was further subjected to iterative cycles of restrained refinement and manual model building with Refmac5, Phenix and Coot (32). In the final structure, three (HMfB)₂ dimers form a protein core that binds one 90 bp DNA molecule (88 bp + 2 nt 5'-extension). The stereochemistry of the final model was evaluated by PROCHECK (33) and MolProbity (34). The data collection and refinement statistics are tabulated in Table S1. Figures were made with Pymol (The PyMOL Molecular Graphics System, Version 1.2r3pre, Schrödinger, LLC.). Electrostatic surfaces were calculated with CCP4mg (35).

Micrococcal Nuclease digestion of in vitro reconstituted HTkA-DNA complexes.

Increasing amounts of HMfB or HTkA dimers were incubated with 147 bp and 207 bp DNA molecules, derived from the '601' nucleosome positioning sequence (36), in 100 mM KCl and 50 mM Tris-HCl (pH 8.0), at room temperature for 20 min. Aliquots of the complexes formed were visualized by staining after electrophoresis through 5% TBE polyacrylamide gels. With the desired HFDs:DNA ratios identified, reaction mixtures (100 μ l) containing 200 nM DNA were assembled. Aliquots (30 μ l) were diluted to a final 100 μ l volume in MNase buffer (50 mM Tris-HCl pH 7.9, 5 mM CaCl₂) that contained BSA (0.1 mg/ml) and 15 U of micrococcal nuclease (MNase, NEB). Control reaction mixtures lacked MNase. After incubation at 37° C for 12 min, the digestion was stopped by addition of 25 μ l of 0.5 M EDTA. Proteinase K (20 μ g) was added and the samples incubated at 50°C for 30 min. A 621 bp DNA loading control (250 nM) was added and the DNA molecules present purified using the MinElute QIAGEN kit and then visualized by staining following their separation by electrophoresis through 10% TBE polyacrylamide gels.

Analytical ultra-centrifugation (AUC). Complexes were prepared at a 1:5 and 1:7 DNA:HTkA HFDs ratio with the 147 bp and 207 bp DNAs, respectively in 50 mM Tris-HCl (pH 8.0), 100 mM KCl buffer, a concentration of 400 nM. The samples were sedimented in an An 60 Ti rotor in a Beckman XL-A centrifuge at 30000 rpm at 20°C. Protein-free 147 bp and 207 bp DNA molecules and salt-assembled nucleosomes (on 147 bp DNA) were run as controls. Absorbance at 260 nm was monitored and the data was analyzed using UltraScan III (37, 38). Molecular weights were calculated using the Genetic Algorithm–Monte Carlo method (GA-MC), using a standard \bar{v} value determined by the UltraScanIII software based on the protein and DNA sequences.

Growth of *Thermococcus kodakarensis*. Cultures of *T. kodakarensis* were maintained anaerobically at 85°C in sealed-vessels with an initial headspace composition of 95% N₂, 5% H₂ (1 bar at 22°C). Growth was followed by OD₆₀₀ measurements. Cultures were grown at 85°C in artificial seawater (ASW) supplemented with 0.5% (w/v) tryptone, 0.5% (w/v) yeast extract, trace mineral solution and vitamin mixture (nutrient rich medium) or with amino acid mixture, trace mineral solution and vitamin mixture (minimal defined medium). ASW contains, per l, 20 g NaCl, 3 g MgCl₂·6H₂O, 6 g MgSO₄·7H₂O, 1 g (NH₄)₂SO₄, 200 mg NaHCO₃, 300 mg CaCl₂·2H₂O, 0.5 g KCl, 420 mg KH₂PO₄, 50 mg NaBr, 20 mg SrCl₂·6H₂O, and 10 mg Fe(NH₄)₂(SO₄)₂·6H₂O. The trace mineral solution (1000x) contains, per l, 0.5 g MnSO₄·6H₂O, 0.1 g CoCl₂·6H₂O, 0.1 g ZnSO₄·7H₂O, 0.01 g CuSO₄·5H₂O, 0.01 g AlK(SO₄)₂·12H₂O, 0.01 g H₃BO₃, 0.01 g Na₂MoO₄·2H₂O. The vitamin mixture (200x) contains, per l, 0.2 g niacin, 0.08 g biotin, 0.2 g pantothenate, 0.2 g lipoic acid, 0.08 g folic acid, 0.2 g p-aminobenzoic acid, 0.2 g thiamine, 0.2 g riboflavin, 0.2 g pyridoxine, 0.2 g cobalamin. The amino acid mixture (20x) contains, per l, 5 g each of cysteine, glutamic acid and glycine, 2.5 g each of arginine and proline, 2 g each of asparagine, histidine, isoleucine, leucine, lysine, threonine, serine and tyrosine, 1.5 g each of alanine, methionine, phenylalanine and tryptophan, and 1 g each of aspartic acid, glutamine, and valine. When present, sodium pyruvate was added at 5 g per l, agmatine sulfate to 1 mM and 6-methyl purine (6MP) to 100 μ M. Elemental sulfur (S°) was added at 2 g per l in liquid media, but was replaced by polysulfide in solid media. Polysulfide solution (500x) contained, per l, 66.7 g sodium sulfide (Na₂S·9H₂O) and 3 g sulfur. Gelrite was added to 1% (w/v) to solidify media.

All growth curves reported here were of cultures inoculated with a 1:100 dilution of a culture of the strain grown to saturation in rich medium containing agmatine and S°. To obtain

sufficient biomass for chromatin preparations from *T. kodakarensis* TS620 and TS621 (Table S3), cells from ~30 to 40 l of culture medium were harvested at an OD₆₀₀ of ~0.4.

Strain construction. *T. kodakarensis* TS600 was constructed using standard techniques (20) from strain TS559 (39) by marker-less deletion of TK2289 (HTkB) (Fig. S5A). Otherwise isogenic derivatives of TS600 with changes in TK1413 that encode HTkA variants with amino acid replacements at G17, E19, and/or G52 were generated by allelic substitution (Fig. S5B) and confirmed by PCR amplification and sequencing, as previously described (20). Despite repeated attempts, and consistent with previous studies of HMfB (40), we were unable to isolate *T. kodakarensis* strains with mutations that would direct the synthesis of HTkA variants (R20S and T55L) with minimal DNA affinity. Construction of strains TS627 and TS628 (Table S3) with silent mutations at these positions confirmed that changing the encoding codons was possible.

qRT-PCR. Cultures of *T. kodakarensis* were harvested at OD₆₀₀ ~0.2. Total RNA was extracted using the TRIZOL reagent (Invitrogen) and cDNA was prepared using the QuantiNova reverse transcription kit (QIAGEN). qRT-PCR was performed on a C1000 thermocycler with a CFX96 detection system using the QuantiNova SYBR Green PCR kit (QIAGEN). The amounts of transcripts of TK2080, TK2081, TK2088 (encoding components of the MBH operon) were calculated by: $2^{-\Delta\Delta C_T}$ and were normalized to transcripts of three constitutively expressed reference genes (TK0895, TK1431, TK1311) using the Bio-rad CFX Manage software (version 2.0). The amounts of TK2080, TK2081, TK2088 transcripts from TS600 (HTkA) samples were normalized to a TS600 sample grown in S^o-containing media, and transcript amounts from TS621 (HTkA G17L) were normalized to a TS621 sample grown in S^o-containing media.

Micrococcal nuclease (MNase) digestion of *T. kodakarensis* chromatin. Cell paste (0.5 g) was ground to a fine powder in a pre-chilled mortar in 10 ml NP40 lysis buffer [10 mM Tris·HCl (pH 7.5), 10 mM NaCl, 3 mM MgCl₂, 0.5% NP40, 0.15 mM spermine, 0.5 mM spermidine]. The powder was transferred to a 50 ml conical tube and allowed to thaw at 37 °C; the freeze-grind-thaw process was then repeated. The lysate was clarified by centrifugation at 1700 g for 5 min. MNase (6000 U, NEB) was added to 500 µl of the resulting supernatant and 50 µl aliquots were taken after 0, 10, 30, 60 and 180 min incubation at 37° C. The reactions were immediately stopped by adding a final concentration of 1% SDS and 25 mM EDTA and stored on ice. DNA was isolated using a QIAquick PCR clean up kit (Qiagen, 28106), its concentration determined by A₂₆₀ measurement, and 0.2 to 0.4 µg were subjected to electrophoresis through a 10% acrylamide gel, run at room temperature in TBE buffer at 200 V for 50 min. The DNA was stained with ethidium bromide and the gels photographed and quantified using a Bio-Rad imaging system with Quantity One (6.6.9) software. For each time point, 5 ng of DNA was run on a DNA1000 chip on an Agilent 2100 Bioanalyzer for sizing and quantification (41).

Histone extraction from *T. kodakarensis*. Cells were lysed as described above. To 4 ml of the supernatant, 20% w/v final concentration sucrose and 3 mM MgAc were added, centrifuged at 10,000 g for 10 min at 4 °C, the supernatant removed and the pellet resuspended in 40 to 60 µl of lysis buffer. Aliquots of the lysate, supernatant and pellet were subjected to SDS denaturing electrophoresis through 15% polyacrylamide gels or 4 to 12% bis-tris criterion XT gels (Bio Rad) run at 200 V for 42 min. Protein bands in the gels were stained with Coomassie brilliant blue.

Identification and quantification of HTkA and HTkA variants in cell lysates. Proteins in cell lysates were separated by electrophoresis through 4-12% SDS gels (as described above) and the regions containing polypeptides ranging from 1 to 15 kDa were excised. The proteins in

these gel fragments were digested with either Lys-C endoproteinase or sequencing grade modified trypsin (Promega), as described (42), and aliquots (5 μ l) of the resulting tryptic peptides were loaded directly onto a Waters nanoACQUITY UPLC BEH C18 column (130 \AA , 1.7 μ m \times 75 μ m \times 250 mm) equilibrated with 0.1% formic acid/3% acetonitrile/water for UPLC-MS/MS analysis. The mobile phase A was 0.1% formic acid/water, phase B was 0.1% formic acid/acetonitrile and elution was at 0.3 μ l/min using gradients of 3 to 8% B (0-5 min) and 8 to 35% B (5-123 min).

MS/MS was performed on a LTQ Orbitrap Velos mass spectrometer, scanning precursor ions between 300 and 1800 m/z (1×10^6 ions, 60,000 resolution) and selecting the 10 most intense ions for MS/MS with 180s dynamic exclusion, 10 ppm exclusion width, repeat count = 1, and 30 s repeat duration. Ions with unassigned charge state and MH^{+1} were excluded from the MS/MS. Maximal ion injection times were 500 ms for FT (one microscan) and 250 ms for LTQ, and the AGC was 1×10^4 . The normalized collision energy was 35% with activation Q 0.25 for 10 ms.

Data analysis. Raw data files from MS were searched against the Uniprot *T. kodakarensis* proteome database (downloaded 1/25/2015; total 2,309 entries) plus the two HTkA variant sequences, using the MaxQuant/Andromeda search engine (version 1.5.2.8) (43, 44). Searches allowed either LysC or trypsin specificity with two missed cleavages, and included fixed Cys carbamidomethylation, and variable acetylation (protein N-terminus) and Met oxidation. Mass tolerances were set to 20 ppm (first search) and 4.5 ppm (main search) for precursor ions, and 0.5 Da for ITMS MS/MS ions. MaxQuant/Andromeda used the top 8 MS/MS peaks per 100 Da and seven amino acid minimum for peptide length, with 0.01 false discovery rate for both protein and peptide identification. Label-free quantification was also used, with 2 minimum ratio counts. MaxQuant/Andromeda output are shown in Table S4.

Supplementary Figures

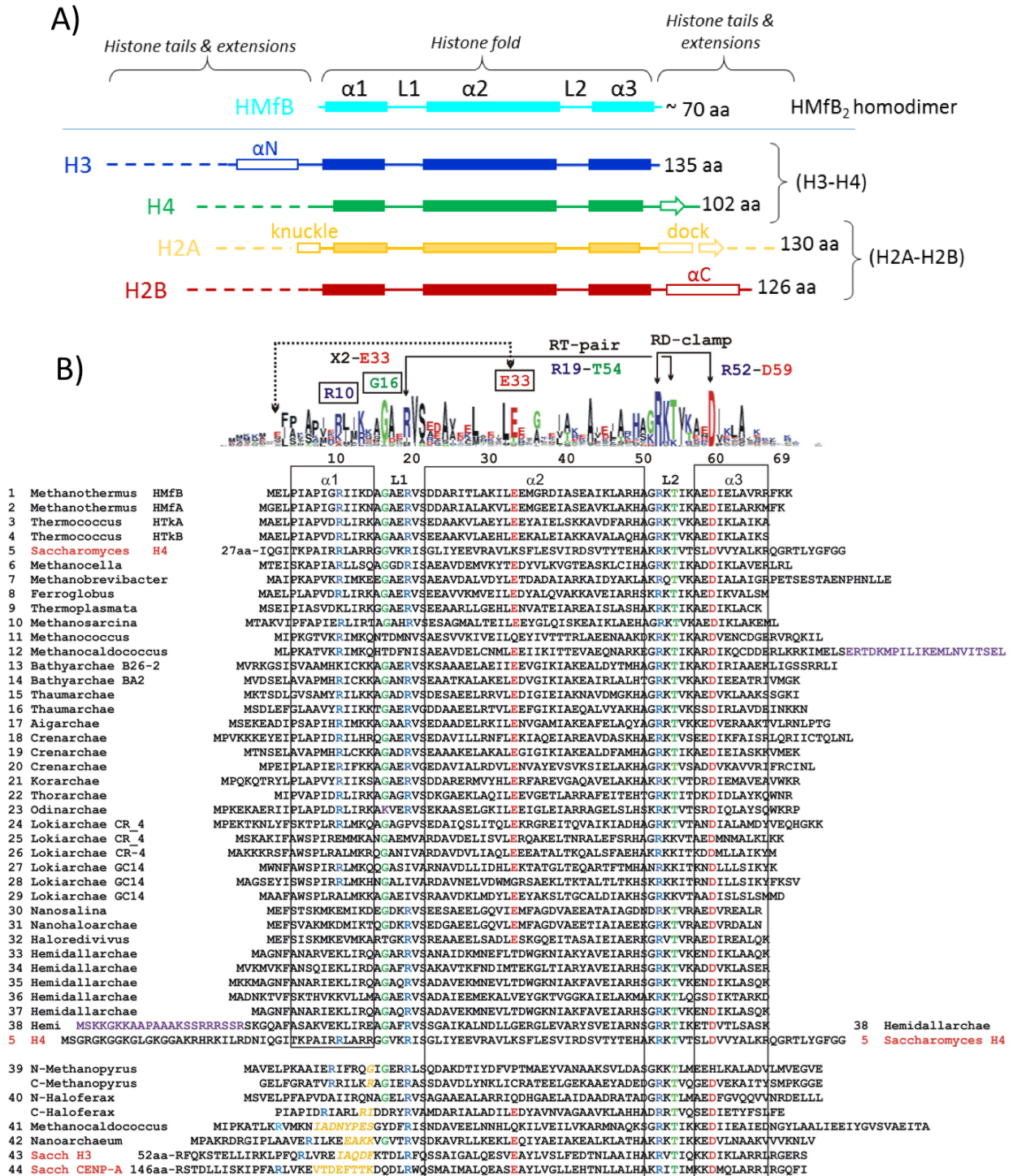


Fig. S1. Structures and alignment of histone fold (HF) sequences. A) The archaeal histone HMfB consists of just the HF (α 1-L1- α 2-L2- α 3) whereas the HF of the four eukaryotic core histones is flanked by divergent N- and/or C-terminal extensions. Dimerization partners are indicated. B) Alignment of HF sequences. The sequences of the archaeal histones, HMfB (#1)

from *Methanothermobacter thermophilus* and HTkA (#3) from *Thermococcus kodakarensis*, used in this study, are shown aligned with the eukaryotic *Saccharomyces cerevisiae* histone H4 sequence (#5) and archaeal histone sequences from each of the recognized archaeal phyla (5, 45). Conserved residues, discussed in the text, are colored with the 'RT-pair' and 'RD-clamp' indicated. The LOGO plot was generated from the archaeal sequences numbered 1 to 4 and 6 to 38. Purple residues identify the C-terminal extension of a Methanocaldococcal histone (#12), and the N-terminal extension of the Hemidallarchaeal histone (#38) that is similar and aligned with the corresponding region of eukaryotic histone H4 (#5). Archaeal histones from *Methanopyrus* (#39) and *Haloferax* (#40) have two covalently linked HFs (46, 47) that are shown with the N-terminal (N-) and C-terminal (C-) HFs aligned separately. Archaeal histones (#39 to #42) have additional residues (colored orange) in loop1 that are aligned with the corresponding regions of *Saccharomyces cerevisiae* histones H3 (#43) and CENP-A (#44). The NCBI reference sequence designations are #1 *Methanothermobacter thermophilus* WP_013414263; #2 *Methanothermobacter thermophilus* WP_013413995; #3 *Thermococcus kodakarensis* WP_011250364; #4 *Thermococcus kodakarensis* WP_011251239; #5 *Saccharomyces cerevisiae* histone H4 NP_009563; #6 *Methanocella* BAI60563; #7 *Methanobrevibacter* ADC47610; #8 *Ferroplasma* WP_02966277; #9 *Thermoplasma* KYK38613; #10 *Methanosarcina* WP_048125684; #11 *Methanococcus* WP_011973395; #12 *Methanocaldococcus* WP_010871171; #13 *Bathyarchae* B26-2 KYH40538; #14 *Bathyarchae* BA2 KPV63666; #15 *Thaumarchae* (*Nitrosopelagicus*), WP_04104690; #16 *Thaumarchae* (*AD1000*) AIE90726; #17 *Aigarchae* (*Caldiarchoaeum*) BAJ48508; #18 *Crenarchae* KON33214; #19 *Crenarchae* (*Thermofilum*) WP_052884954; #20 *Crenarchae* (*Caldivirga*) WP_012186746; #21 *Korarchae* WP_012308704.1; #22 *Thorarchae* KXH71038; #23 *Odinarchae* OLS18261; #24 *Lokiarchae* CR_4 OLS16336; #25 *Lokiarchae* CR_4 OLS15619; #26 *Lokiarchae* CR-4 OLS12771; #27 *Lokiarchae* GC14 KKK44894; #28 *Lokiarchae* GC14 KKK41688; #29 *Lokiarchae* GC14 KKK45508; #30 *Nanosalina* EGQ43804; #31 *Nanohaloarchae* AOV94489; #32 *Haloredivivus* EHK02195; #33 *Hemidallarchae* OLS26110; #34 *Hemidallarchae* OLS24625; #35 *Hemidallarchae* OLS19133; #36 *Hemidallarchae* OLS18443; #37 *Hemidallarchae* OLS19133; #38 *Hemidallarchae* OLS22331; #39 *Methanopyrus* AAC72546; #40 *Haloferax* WP_008091782; #41 *Methanocaldococcus* WP_015792102; #42 *Nanoarchaeum* AAR39136; #43 *Saccharomyces cerevisiae* histone H3 NP_009564; #44 *Saccharomyces cerevisiae* CENP-A CAA81884.

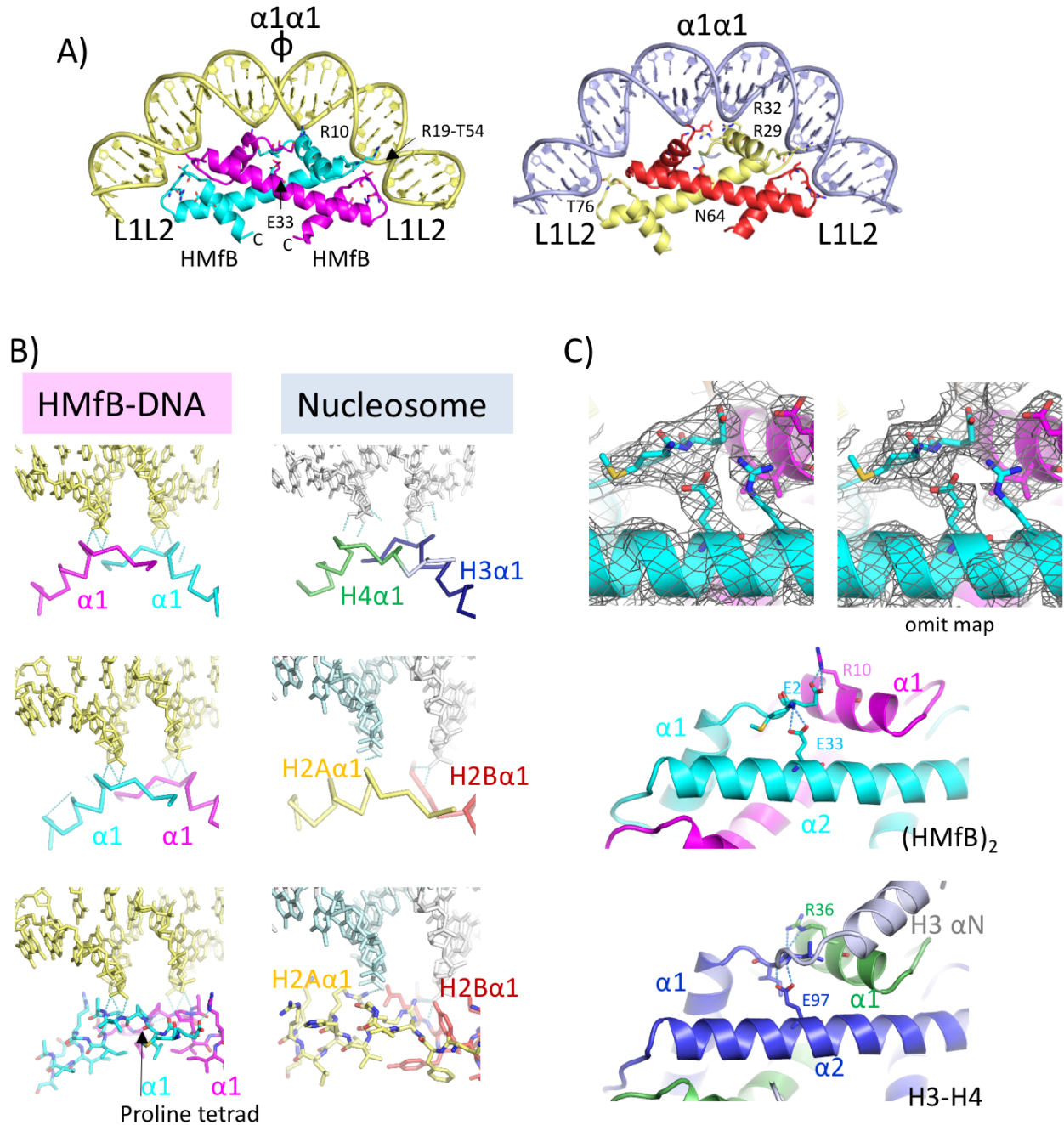


Fig. S2. Histone-DNA interactions in HMfB-chromatin resemble those observed throughout the nucleosome. **A)** The HMfB HFD and associated DNA is structurally similar to the H2A-H2B dimer in the nucleosome. **B)** $\alpha1\alpha1$ interfaces in HMfB, H3-H4, and H2A-H2B are similar in their main chain geometry, but differ in details of the interactions. Two prolines, P4 and P7, form a proline tetrad in the (HMfB)₂ dimer which was predicted to be a defining feature of archaeal histone assembly and DNA binding (10), but this is not the case. Although the N-terminus of $\alpha1$ is often established by a proline, prolines are not universally conserved at these locations (Fig. S1B), and P4 and P7 of HMfB do not contact the DNA. **C)** E33 stabilizes the N-terminus of HMfB. 1σ 2Fo-Fc electron density and 1σ simulated annealing 2Fo-Fc omit map are shown (top panels), together with a comparison of HMfB (middle panel) and the equivalent region in H3-H4 (bottom

panel), where this interaction serves to stabilize the trajectory of αN (grey). A similar arrangement is observed in H2A (not shown). The omit map was generated with Phenix using the simulated annealing procedure.

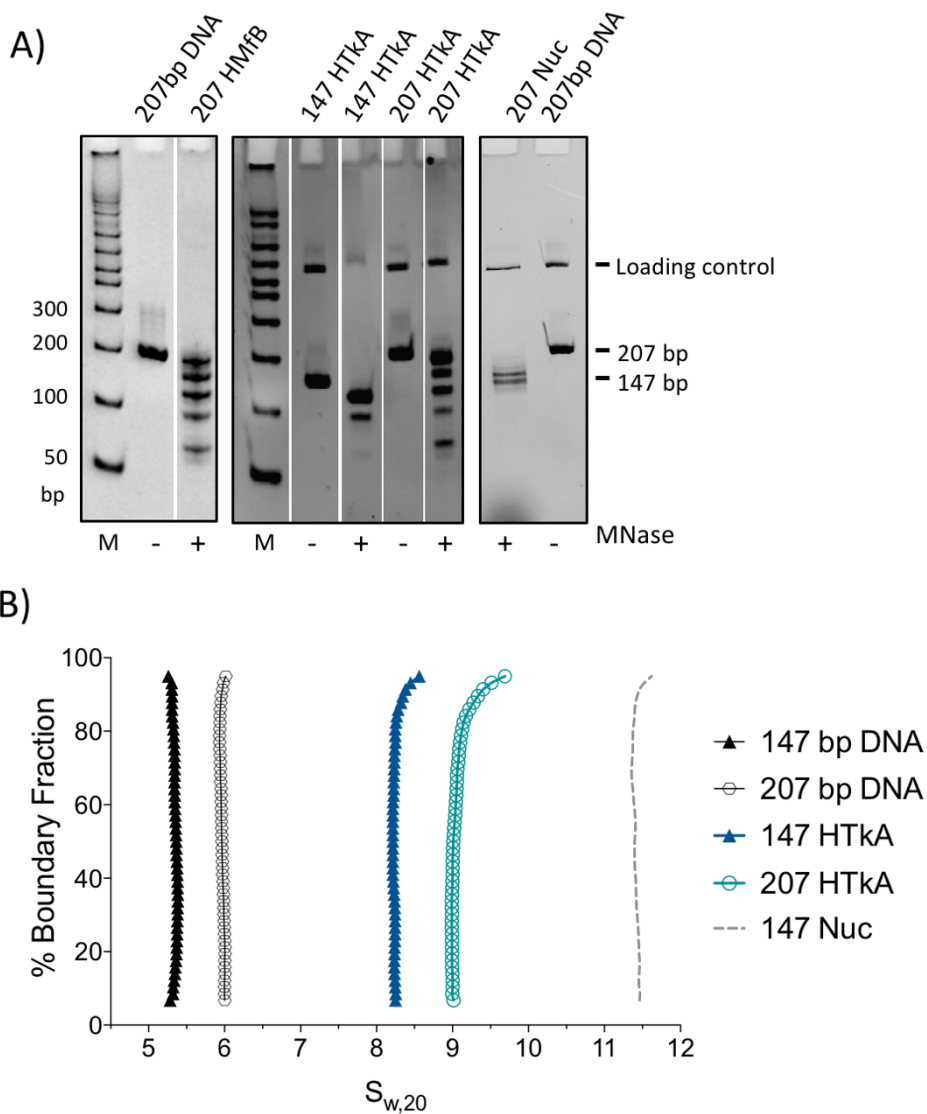


Fig. S3: HMfB and HTkA assemble into long superhelical structures on 147 and 207 bp DNA. **A)** MNase digestion of in vitro assembled HMfB- and HTkA-DNA complexes on 147 bp or 207 bp DNA molecules. Nuclease digestions were carried out on 60 nM aliquots with 15 U of enzymes at 37 °C for 12 min. The purified DNA fragments were visualized by staining after separation by electrophoresis through 10% polyacrylamide gels run in TBE buffer. **B)** Van Holde-Weischet plots of AUC experiments with archaeal histone dimers assembled on 147 bp (dark blue) and 207 bp DNA molecules (light blue) show homogenous complex formation, as visualized by the straight line boundary fraction curves obtained for each sample. Analysis of the sedimentation velocities was used to calculate the masses of the complexes shown in Table S2. Protein-free DNA molecules and in vitro assembled eukaryotic nucleosomes were included as controls. Modeling and energy minimization performed using phenix and Coot confirmed that extended polymerization is also compatible with the assembly of homodimers of HMfA, the second histone present in *M. fervidus*, of (HMfA+HMfB) heterodimers, and of (HTkA)₂ and (HTkB)₂ dimers from *Thermococcus kodakarensis* (Fig. S1B).

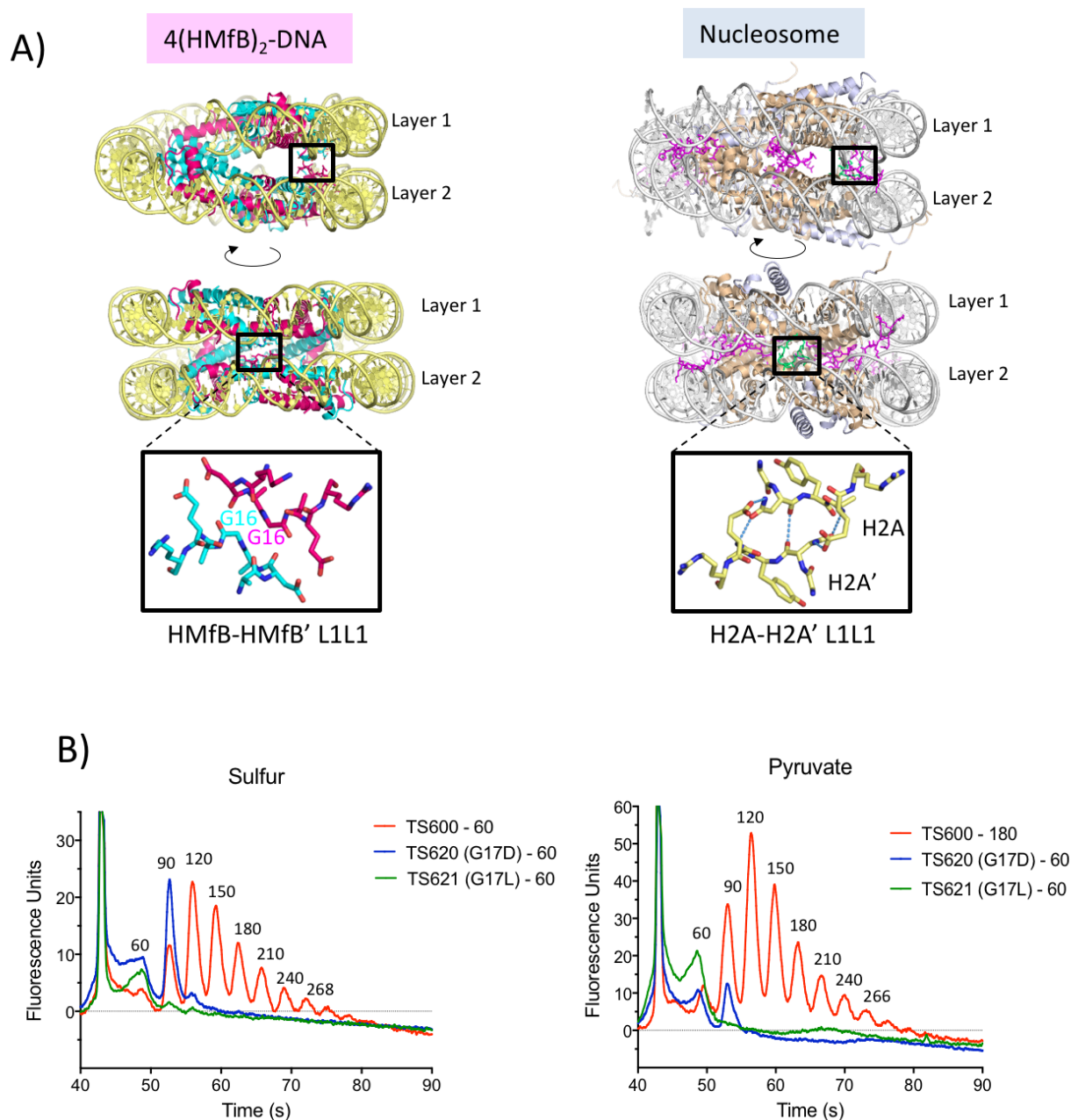


Fig. S4: Disturbance of layer interfaces affects chromatin structure in *T. kodakarensis*. **A)** Side views of an HMfB octamer (left panel) and histone octamer (right panel) with DNA, shown in two orientations (rotated around the y axis). In the nucleosome, histone fold extensions (H2A docking domain, H2B N-terminal tail, and H4 C-terminal tail; all shown with side chains in magenta) stabilize the two layers; features not present in HMfB. The close proximity of the two L1 loops from the two histone monomers between the two layers of HMfB-chromatin and of the nucleosome is indicated (inset); the conserved glycine (G16 in HMfB, G17 in HTkA; Fig. S1B) is labeled. The side chains of the amino acids flanking G16 point away from the interface and do not contribute to the interaction. **B)** Electropherograms of DNA fragments generated by MNase digestion of chromatin from *T. kodakarensis* TS600, TS620 (G17D) and TS621 (G17L) strains

shown in Fig. 3C. Peak height provides a measure of the relative amounts of the different sized fragments, and peak position correlates with length, ± 5 bp for 25 to 100 bp fragments; $\pm 5\%$ for 100 to 500 bp fragments.

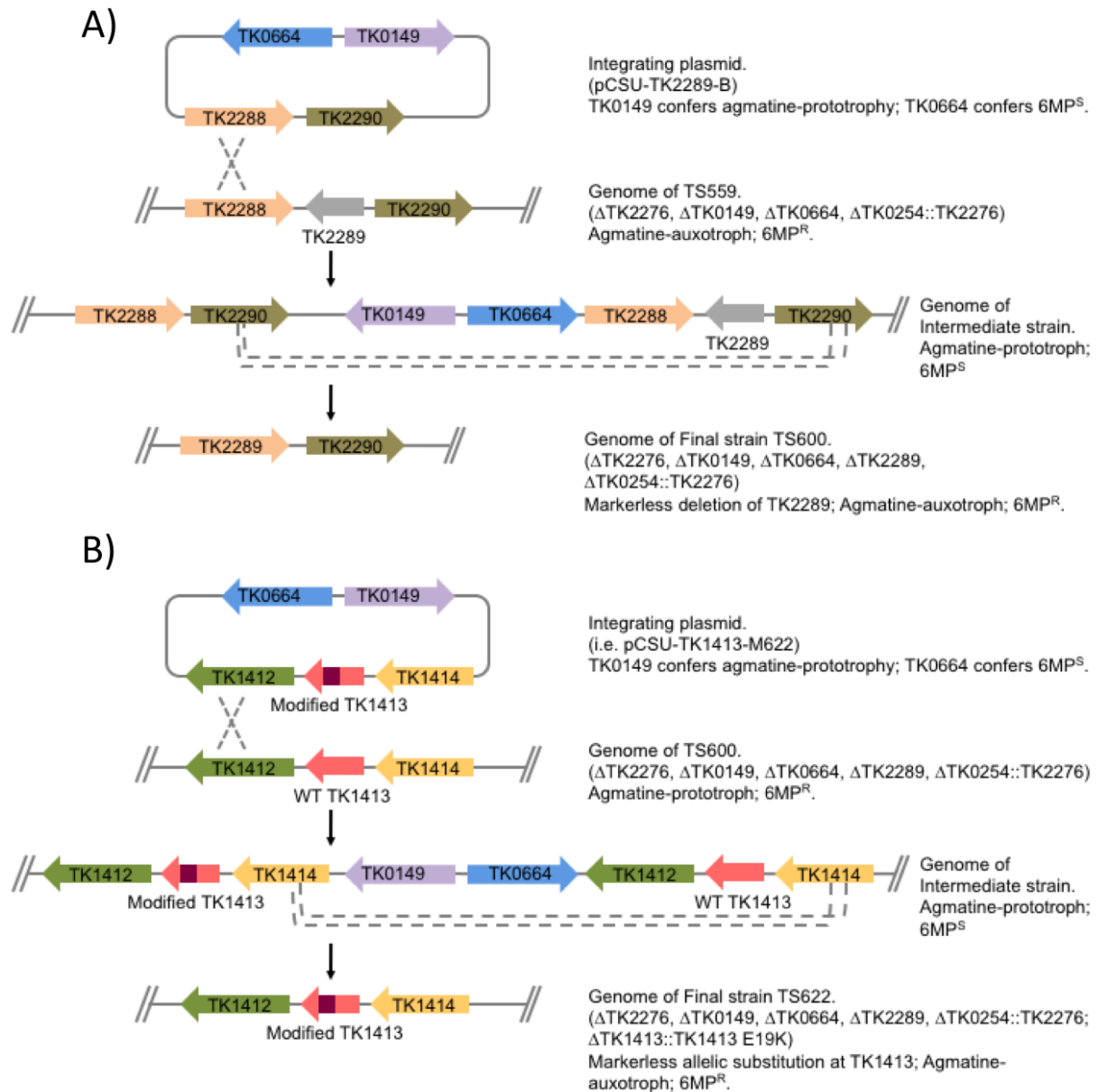


Fig. S5: Construction of *T. kodakarensis* strains encoding single and variant HTkA proteins. Established genetic techniques (20, 39) permit initial integration and subsequent excision of donor DNAs [pCSU-TK2289-B (A) and pCSU-TK1413-M622 (B)] into the genome of strains TS559 (A) or TS600 (B), respectively. Integration of donor plasmids is directed by homologous recombination to the desired genomic locus; integration confers both agmatine prototrophy and 6-methyl purine sensitivity (6-MP^S) on intermediate strains. Following confirmation of the desired genomic integration via diagnostic PCR (20), intermediate strains are exposed to a 6-MP based counter-selection, selecting for cells that have spontaneously excised the donor DNA while simultaneously deleting TK2289 (A) or introducing an allelic substitution into TK1413 (B).

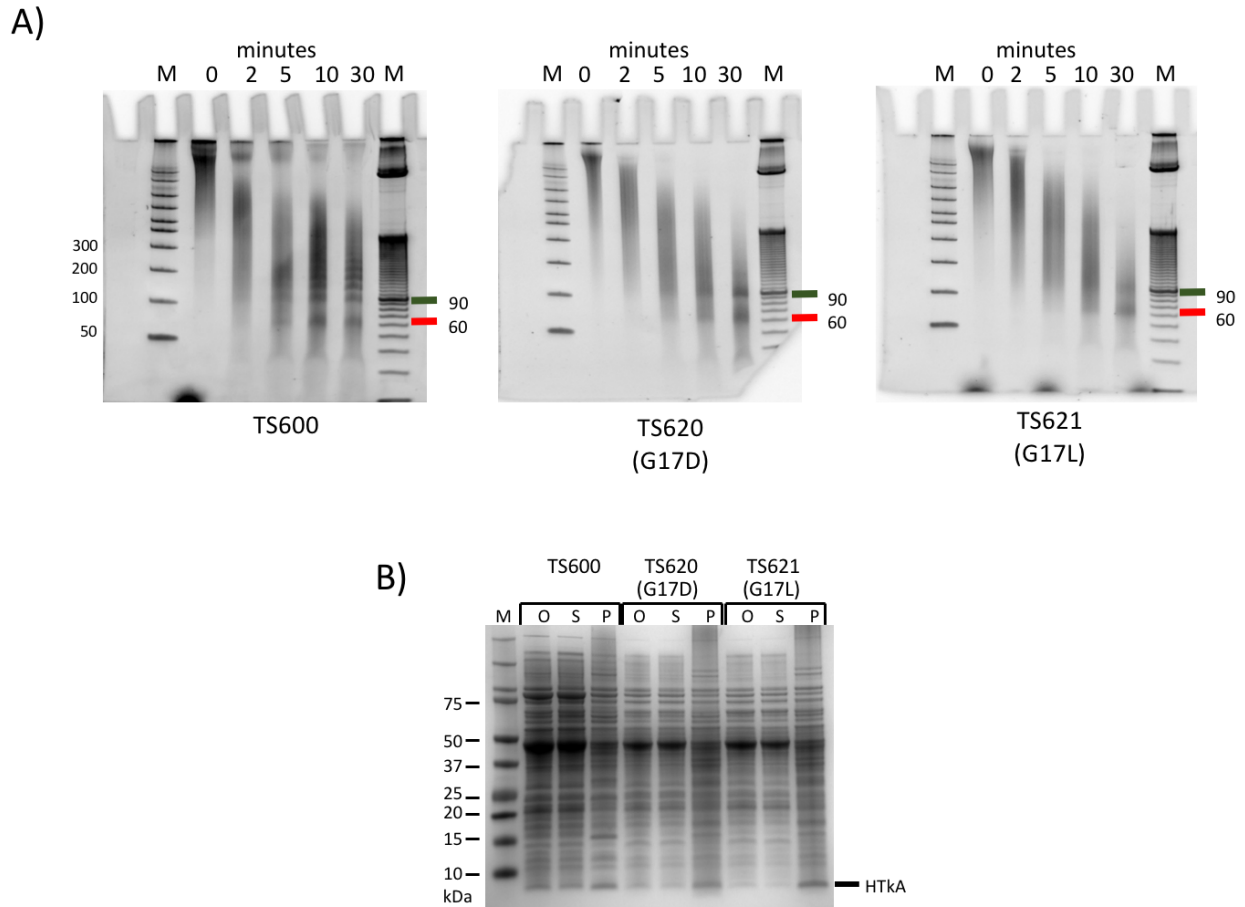


Fig. S6: HTkA histone mutants are expressed in *T.kodakarensis* but result in altered chromatin structure. A) DNA fragments generated by MNase digestion of chromatin isolated from *T. kodakarensis* strains TS600, TS620 (HTkA G17D), and TS621 (HTkA G17L) grown in S⁰-containing media. Size standards are in lanes M. B) SDS-PAGE separation of proteins present in lysates (O), the soluble (S) and insoluble (P) fractions of cells isolated at the same growth stage from cultures of *T. kodakarensis* strains TS600 (HTkA), TS620 (HTkA G17D), and TS621 (HTkA G17L). The histones were present predominantly in the insoluble fraction, pelleted with DNA.

Supplementary Tables

Table S1: Data collection and refinement statistics.

Data Set	Final	Initial
Data collection		
Wavelength (Å)	1.5418	1.5418
Space group	P6 ₅	P6 ₂₂
Unit cell dimensions		
a, b, c (Å)	99.45, 99.45, 171.73	99.49, 99.49, 171.76
α , β , γ	90°, 90°, 120°	90°, 90°, 120°
Resolution	19.76-4.0 (4.22-4.0)	19.77-3.99 (4.21-3.99)
Total number of observations	93771 (13330)	94787 (13793)
Number of unique reflections	8122 (1183)	4634 (650)
Completeness (%)	99.2 (100.0)	99.2 (99.7)
Multiplicity	11.5 (11.3)	20.5 (21.2)
Mean ($I/\sigma(I)$)	19.9 (5.7)	25.8 (7.5)
R_{merge}^a	0.145 (0.517)	0.149 (0.573)
R_{pim} (within I+/I-)	0.044 (0.159)	0.033 (0.125)
R_{pim} (all I+ & I-)	0.044 (0.159)	0.033 (0.125)
CC1/2	0.999 (0.928)	
Refinement		
Resolution limits	19.76 – 4.019	
No. of used reflections	8070	
No. of reflections for R_{free}	373	
Solvent content (%)	47.2	
R_{work}^b (%)	21.4	
R_{free}^c (%)	26.2	
No. of atoms in ASU		
Macromolecules	6816	
Ligand	15	
Average B factors (Å ²)	113	
Protein	80	
DNA	141	
Ligand	96	
R.M.S.D. ^d from ideal		
Bond lengths (Å)	0.003	
Bond angles (°)	0.537	
Ramachandran plot		
Preferred region (%)	97.7	
Allowed region (%)	2.3	
Outliers (%)	0.0	

^a $R_{merge} = \sum_{hkl} \sum_i |I_i(hkl) - \langle I(hkl) \rangle| / \sum_{hkl} \sum_i I_i(hkl)$; $I_i(hkl)$ is the observed intensity of a i -th reflection and $\langle I(hkl) \rangle$ is the mean value for all equivalent measurement of reflection hkl .

^b $R_{work} = \sum_{hkl} ||F_{obs}| - |F_{calc}|| / \sum |F_{obs}|$; F_{obs} and F_{calc} are the observed and calculated structure factor.

^c R_{free} is calculated in the same way as R_{work} , based on 5% of total reflections excluded from refinement.

^d R.M.S.D., root mean square deviation

Table S2: Analytical ultracentrifugation results. Expected and measured values derived from the AUC experiments shown in Fig. S3B. The data were analyzed in UltraScanIII and the molecular weight estimation is based on a \bar{v} calculated by the software based on DNA and protein sequence.

Sample	$s_{20,w}$ value	expected MW	measured MW	DNA:HFDs	f/f0
				measured ratio	
147 DNA	5.4	90.7	107	NA	2.7
207 DNA	6.0	127.8	150	NA	3.1
147 Nuc	11.4	199.7	196	NA	1.4
147 HTkA	8.2	163.2	167	1:5	1.8
207 HTkA	9	229.3	214	1:6	2

Table S3: Growth parameters of *T. kodakarensis* strains. Full genotypes of the strains employed are listed with their calculated lag- and doubling-times. Lag-periods were the time before exponential growth began, and doubling times were calculated from the $\ln(2)$ of the optical density values at maximal exponential growth. Values for TS559 were set to 100% or 1X and the values in parentheses for all other strains reflect their relationship to TS559 values. Growth parameters from +S° and -S° (pyruvate) grown cultures are in green and blue, respectively, with values that differ significantly from the TS559 values highlighted in red. Although not the case for all *Euryarchaea*, *T. kodakarensis* viability is dependent on the presence of an archaeal histone that is able to bind DNA. Strains could be constructed with HTkA variants (E19K, G52K or E19K+G52K) that had increased DNA binding ability, but all attempts to introduce substitutions into HTkA that substantially reduced DNA binding (R20S and T55L) were unsuccessful. Silent allelic substitutions are tolerated at R20 and T55 of HTkA (TS627 and TS628, respectively), however we could not isolate strains with substitutions in HTkA (R20S or T55L) that dramatically reduce the affinity of HTkA for DNA (40). A growth curve for TS559 (*) is not present in Fig. 3A.

Strain	Genotype	Sulfur			Pyruvate		
		Lag phase	Max OD _{600 nm}	Doubling time	Lag phase	Max OD _{600 nm}	Doubling time
TS559*	Δ TK0149; Δ TK0664; Δ TK2276; Δ TK0254::TK2276	0 hours	0.58 (100%)	120 min (1.0X)	4 hours	1.30 (100%)	130 min (1.0X)
TS600	TS559; Δ TK2289	0 hours	0.57 (98%)	120 min (1.0X)	4 hours	1.27 (98%)	130 min (1.0X)
TS616	TS600; TK1413::TK1413 ^{G17G}	0 hours	0.56 (97%)	120 min (1.0X)	4 hours	1.32 (102%)	130 min (1.0X)
TS617 (G17H)	TS600; TK1413::TK1413 ^{G17H}	0 hours	0.70 (120%)	120 min (1.0X)	11 hours	1.22 (94%)	130 min (1.0X)
TS618 (G17N)	TS600; TK1413::TK1413 ^{G17N}	0 hours	0.54 (93%)	120 min (1.0X)	9 hours	1.21 (93%)	120 min (0.9X)
TS619 (G17S)	TS600; TK1413::TK1413 ^{G17S}	0 hours	0.45 (78%)	120 min (1.0X)	15 hours	0.60 (46%)	330 min (2.5X)
TS620 (G17D)	TS600; TK1413::TK1413 ^{G17D}	0 hours	0.44 (76%)	120 min (1.0X)	15 hours	0.15 (11.5%)	1300 min (10X)
TS621 (G17L)	TS600; TK1413::TK1413 ^{G17L}	0 hours	0.60 (103%)	120 min (1.0X)	10 hours	0.59 (45%)	620 min (4.8X)
TS622 (E19K)	TS600; TK1413::TK1413 ^{E19K}	0 hours	0.52 (90%)	130 min (1.1X)	4 hours	1.11 (85%)	140 min (1.1X)
TS623 (G52K)	TS600; TK1413::TK1413 ^{G52K}	0 hours	0.66 (114%)	110 min (0.9X)	4 hours	1.15 (88%)	130 min (1.0X)
TS626 (E19K/G52K)	TS600; TK1413::TK1413 ^{E19K/G52K}	0 hours	0.57 (98%)	120 min (1.0X)	4 hours	1.02 (78%)	180 min (1.4X)
TS627	TS600; TK1413::TK1413 ^{R20R}	0 hours	0.58 (100%)	120 min (1.0X)	4 hours	1.33 (102%)	130 min (1.0X)
TS628	TS600; TK1413::TK1413 ^{T55T}	0 hours	0.56 (97%)	120 min (1.0X)	4 hours	1.33 (102%)	130 min (1.0X)

Table S4: Identification of HTkA, HTkA G17D and G17L variants in lysates of cells removed from esponentially growing cultures of *T. kodakarensis*. Search results for peptides corresponding to amino acids 15-26 of HTkA in each sample. All the peptides identified had high scores and characteristic b- and y- ions confirming the desired amino acid substitutions at G17. This analysis also confirmed that these strains had only one archaeal histone, exclusively HTkA, HTkA G17D or HTkA G17L.

Sequence	Peptide from	MS/MS m/z	charge	Mass	Score	Delta score
¹⁵ AGAERVSEDAAK ²⁶	TS600	401.87	3	1202.58913	105.13	89.127
¹⁵ ADAERVSEDAAK ²⁶	TS620 (G17D)	631.30	2	1260.59461	171.62	171.62
¹⁵ ALAERVSEDAAK ²⁶	TS621 (G17L)	630.83	2	1258.65173	171.99	145.33

Supplementary References

23. M. R. Starich, K. Sandman, J. N. Reeve, M. F. Summers, NMR structure of HMfB from the hyperthermophile, *Methanothermus fervidus*, confirms that this archaeal protein is a histone. *J Mol Biol* **255**, 187-203 (1996).
24. P. N. Dyer *et al.*, Reconstitution of nucleosome core particles from recombinant histones and DNA. *Methods Enzymol* **375**, 23-44 (2004).
25. W. Kabsch, Automatic indexing of rotation diffraction patterns. *J. Appl. Cryst* **21**, 67-72 (1988).
26. P. Evans, Scaling and assessment of data quality. *Acta Crystallogr D Biol Crystallogr* **62**, 72-82 (2006).
27. M. D. Winn *et al.*, Overview of the CCP4 suite and current developments. *Acta Crystallogr D Biol Crystallogr* **67**, 235-242 (2011).
28. A. J. McCoy *et al.*, Phaser crystallographic software. *J Appl Crystallogr* **40**, 658-674 (2007).
29. G. N. Murshudov *et al.*, REFMAC5 for the refinement of macromolecular crystal structures. *Acta Crystallogr D Biol Crystallogr* **67**, 355-367 (2011).
30. A. Vagin, A. Teplyakov, Molecular replacement with MOLREP. *Acta Crystallogr D Biol Crystallogr* **66**, 22-25 (2010).
31. P. D. Adams *et al.*, PHENIX: a comprehensive Python-based system for macromolecular structure solution. *Acta Crystallogr D Biol Crystallogr* **66**, 213-221 (2010).
32. P. Emsley, K. Cowtan, Coot: model-building tools for molecular graphics. *Acta Crystallogr D Biol Crystallogr* **60**, 2126-2132 (2004).
33. R. A. Laskowski, PDBsum: summaries and analyses of PDB structures. *Nucleic Acids Res* **29**, 221-222 (2001).
34. V. B. Chen *et al.*, MolProbity: all-atom structure validation for macromolecular crystallography. *Acta Crystallogr D Biol Crystallogr* **66**, 12-21 (2010).
35. S. McNicholas, E. Potterton, K. S. Wilson, M. E. Noble, Presenting your structures: the CCP4mg molecular-graphics software. *Acta Crystallogr D Biol Crystallogr* **67**, 386-394 (2011).
36. P. T. Lowary, J. Widom, New DNA sequence rules for high affinity binding to histone octamer and sequence-directed nucleosome positioning. *J Mol Biol* **276**, 19-42. (1998).
37. B. Demeler *et al.*, Characterization of size, anisotropy, and density heterogeneity of nanoparticles by sedimentation velocity. *Anal Chem* **86**, 7688-7695 (2014).
38. G. Gorbet *et al.*, A parametrically constrained optimization method for fitting sedimentation velocity experiments. *Biophys J* **106**, 1741-1750 (2014).
39. T. J. Santangelo, L. Cubonova, J. N. Reeve, *Thermococcus kodakarensis* genetics: TK1827-encoded beta-glycosidase, new positive-selection protocol, and targeted and repetitive deletion technology. *Appl Environ Microbiol* **76**, 1044-1052 (2010).
40. D. J. Soares, F. Marc, J. N. Reeve, Conserved eukaryotic histone-fold residues substituted into an archaeal histone increase DNA affinity but reduce complex flexibility. *J Bacteriol* **185**, 3453-3457 (2003).
41. U. M. Muthurajan *et al.*, In Vitro Chromatin Assembly: Strategies and Quality Control. *Methods Enzymol* **573**, 3-41 (2016).
42. A. Shevchenko, H. Tomas, J. Havlis, J. V. Olsen, M. Mann, In-gel digestion for mass spectrometric characterization of proteins and proteomes. *Nat Protoc* **1**, 2856-2860 (2006).
43. J. Cox, M. Mann, MaxQuant enables high peptide identification rates, individualized p.p.b.-range mass accuracies and proteome-wide protein quantification. *Nat Biotechnol* **26**, 1367-1372 (2008).
44. J. Cox *et al.*, Andromeda: a peptide search engine integrated into the MaxQuant environment. *J Proteome Res* **10**, 1794-1805 (2011).
45. A. Spang *et al.*, Complex archaea that bridge the gap between prokaryotes and eukaryotes. *Nature* **521**, 173-179 (2015).
46. R. L. Fahrner, D. Cascio, J. A. Lake, A. Slesarev, An ancestral nuclear protein assembly: crystal structure of the *Methanopyrus kandleri* histone. *Protein Sci* **10**, 2002-2007 (2001).
47. E. A. Lynch *et al.*, Sequencing of seven haloarchaeal genomes reveals patterns of genomic flux. *PLoS One* **7**, e41389 (2012).